Friction and wear properties of GLC and DLC coatings under ionic liquid lubrication

Mingming Yan [a,b], Xinyu Wang [a,b], Songwei Zhang [a,c], Shuaituo Zhang [a,b,c], Xudong Sui [a,b,c,*], Wensheng Li [d], Junying Hao [a,b,c,**], Weimin Liu [a]

[a] State Key Laboratory of Solid Lubrication, Lanzhou Institute of Chemical Physics, Chinese Academy of Science, Lanzhou, 730000, China
[b] Center of Materials Science and Optoelectronics Engineering, University of Chinese Academy of Sciences, Beijing, 100049, China
[c] Qingdao Center of Resource Chemistry and New Materials, Qingdao, 266000, China
[d] State Key Laboratory of Advanced Processing and Recycling of Nonferrous Metals, Lanzhou University of Technology, Lanzhou, 730050, China

ARTICLE INFO

ABSTRACT

Cr-doped graphite-like carbon (Cr-GLC) coatings and Cr-doped diamond-like carbon (Cr-DLC) coatings were prepared by PVD and PECVD, respectively. The lubrication behaviour of the solid-liquid composite lubrication systems was investigated using two ionic liquids (ILs) as lubricants. The results show that the friction coefficient was reduced by approximately 40% compared with that under the dry condition, and the composite system exhibited a good synergistic lubrication effect. The Cr-DLC coating showed better tribological behaviour than the Cr-GLC coating, which can be ascribed to a better physicochemical film formation under friction and the compact microstructure of the Cr-DLC coating. The synergistic effect of the composite systems was affected by the viscosity and corrosiveness of the ILs and the microstructure of the coatings.

1. Introduction

Amorphous carbon coatings have been widely used in aerospace, microelectronic systems, and other fields [1,2] owing to their excellent mechanical and tribological properties. Carbon is present in the amorphous carbon coatings mainly in the hybridised sp^2 or sp^3 form. The presence of diamond-like or graphite-like structures depends on the sp^2/sp^3 ratio. DLC coatings contain more sp^3-bonded carbon, which has a higher hardness and elastic modulus, resulting in excellent tribological behaviour. Therefore, they can be widely applied in cutting tools, bearings, automobiles, and other applications [3–6]. GLC coatings contain more sp^2-bonded carbon, which results in a self-lubrication effect and high antiwear properties in several applications. They can be used as the working surface for moving parts used in seawater environments [7–9]. Li et al. [10] investigated the load-carrying capacities of DLC, GLC, and CrN coatings under sliding friction in different environments and found that the load-carrying capacity was closely related to the surface roughness, coating thickness, and mechanical properties. Aboua et al. [11,12] studied the friction and wear properties of DLC coatings under boundary lubrication conditions; the results indicated

that carbon diffusion was an important parameter affecting the tribological behaviour of hydrogenated amorphous carbon coatings under boundary lubrication. Fan et al. [13,14] showed that friction-induced graphitisation at the sliding interface was the key condition for obtaining excellent tribological behaviour of Cr-DLC-grease lubricant coatings. Therefore, the tribological behaviour of carbon coatings is affected by many factors, in particular the structure of the carbon coating, so it is useful to study the tribological properties of carbon coatings with various sp^2/sp^3 ratios to further understand the wear mechanism.

Solid lubricants exhibit good antifriction and wear resistance properties. However, long-term stable maintenance of these properties is difficult when the lubricants are subjected to vacuum or heavy loads. Conversely, liquid lubricants can easily reduce the wear loss, but their volatility and strong environmental dependence limit their application. Consequently, traditional single solid or liquid lubricants cannot effectively tolerate the harsh environment of modern equipment. Solid-liquid composite lubrication systems composed of solid coatings and a fluid can effectively combine the advantages and minimise the shortcomings of each component, resulting in a synergistic effect; thus, they have

---

Table 1
Deposition parameters of Cr-GLC and Cr-DLC coatings.

Coating		Cr target (kW)	C target (kW)	Ar (sccm)	C$_4$H$_{10}$ (sccm)	Bias voltage (V)	Deposition technique
GLC	Cr	0.1	0.05	16	–	400	PVD
	Cr–C	1.2	0.3	16	–	60	
	Cr-GLC	0.1	2.0	16	–	60	
DLC	Cr	0.07	–	26	0	400	PECVD
	Cr–C	1.2	–	24	10	40	
	Cr-DLC	0.1	–	21	20	40	

attracted considerable attention. ILs are organic salts consisting of anions and cations; they are polar and have high thermal stability and low sensitivity to environmental changes compared to traditional lubricants [15]. Previous research on the effect of the chain length of the cation, temperature, and lubrication properties on the tribological behaviour has yielded valuable information. Feng et al. [16] studied the tribological properties of Ti-DLC coatings under ILs or perfluoropolyether (PFPE) in a composite lubrication system. The composite system exhibited excellent antifriction performance when the ILs were used, and the friction coefficient was reduced by 47% compared with that when PFPE was used. Tariq et al. [17] investigated the tribological behaviour of gold with different ILs and found that the alkyl chain length of the cation significantly affected the tribological properties. Yao et al. [18] reported that ILs bearing long alkyl side chains have excellent friction-reducing and antiwear properties resulting from the formation of high-quality boundary films during friction. Most importantly, solid-liquid composite lubrication systems consisting of carbon coatings have been widely investigated. However, the effects of two types of carbon coatings (DLCs and GLCs) on the tribological properties of solid-liquid composite lubrication systems are rarely compared. Therefore, the tribological properties of a composite lubrication system of GLC and DLC coatings and the ILs 1-methyl-3-allyl imidazole tetrafluoroborate (LAB103) and 3-methyl-1-butylimidazolium tetrafluoroborate (LB104) are systematically studied in this work.

The Cr-GLC and Cr-DLC coatings were deposited by magnetron sputtering. The tribological properties of the two coatings were investigated using a ball-on-disc tribological tester under a dry condition and under lubrication by LAB103 and LB104, and the wear mechanisms were systematically analysed. The result further illuminates the synergistic lubrication behaviour of Cr-doped amorphous carbon coatings with various sp^2/sp^3 ratios in the presence of an IL.

2. Experimental section

2.1. Material characteristics

Steel (9Cr18, φ25 mm × 8 mm) was used as the substrate in the tribological tests because of its high antiwear performance. A Si(100) wafer was used as the substrate for studying the chemical compositions of the two coatings. The 9Cr18 steel was polished to a mirror surface before deposition. All the substrates were ultrasonically spun in a bath of petroleum ether and absolute alcohol for 15 min.

The Cr-GLC coatings were deposited on the 9Cr18 steel and Si wafer by PVD, and the Cr-DLC coatings were deposited on these substrates by PECVD. There were four target positions in the deposition system, and the vacuum was controlled by a mechanical pumping and molecular pumping system. To remove the oxides, the steel and Si wafers were cleaned by Ar$^+$ bombardment when the vacuum reached 4.0×10^{-4} Pa,
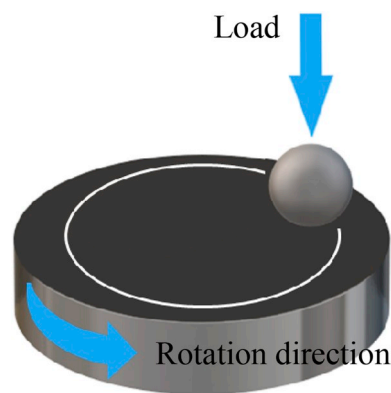
**Fig. 2.** Schematic diagram of the contact mode and direction of rotation during friction.

with a cleaning time of 10 min and a bias voltage of −400 V. To improve the adhesion force, a Cr layer was prepared as a buffer layer. The carbon was provided by a pure graphite target for Cr-GLC coating and by butane for Cr-DLC coating. The detailed deposition parameters are shown in Table 1.

The structural compositions of the ILs are shown in Fig. 1. The anion in both LAB103 and LB104 is BF- 4, and the cations of LAB103 and LB104 differ in that LAB103 has a double bond structure, whereas LB104 has a long chain structure. The viscosity of the LAB103 and LB104 used in this study was 6.11 and 0.14 Pa s at 20 °C, respectively. The contact angles were measured at room temperature to analyse the wettability of the ILs on the two coating surfaces using a contact angle system (OCA20, Dataphysics, Germany).

2.2. Structure and mechanical properties of investigated coatings

Field emission scanning electron microscopy (FE-SEM, JSM-7610F, JEOL, Japan) with energy-dispersive X-ray spectroscopy (EDX) was used to characterise the surface and cross-sectional morphologies as well as the chemical composition of the coatings. The centerline average roughness R_a of the as-deposited coatings on the Si wafer was obtained from a 1 μm × 1 μm area by atomic force microscopy (SPM-9700HT, Shimadzu, Japan). The bonding structure of carbon atoms in the coatings was investigated by Raman spectroscopy (LabRAM HR Evolution, Horiba, France) with an Ar + laser source at 532 nm. X-ray photoelectron spectroscopy (XPS, ESCALAB 250Xi, Thermo Scientific, USA) was applied to analyse the chemical bonding states of the two coatings.

The hardness and elastic modulus were characterised by a Nano Indenter II system (MTS, USA) with an indentation depth of 200 nm, and
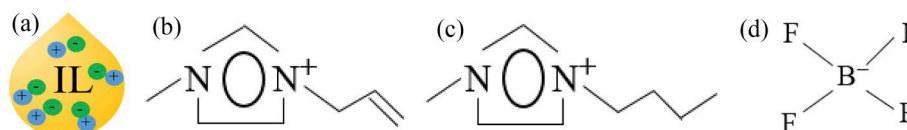
Fig. 1. (a) Structural composition of ILs (b) cation of LAB103 (c) cation of LB104 (d) anion of ILs.
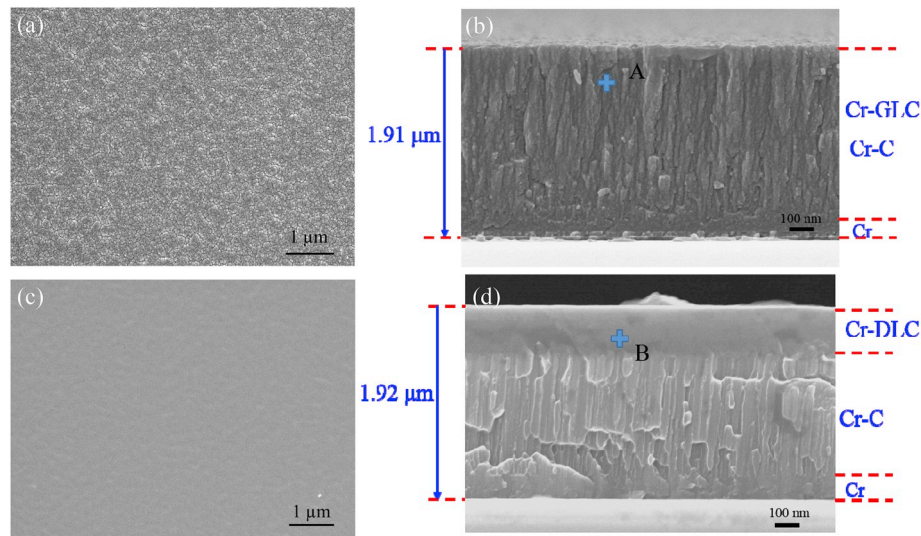
Fig. 3. FESEM images of (a) Cr-GLC coating surface; (b) cross-section of Cr-GLC; (c) Cr-DLC coating surface; (d) cross-section of Cr-DLC.

each sample was measured five times to ensure the reliability of the data. The adhesion force between the coatings and substrates was measured by a scratch tester (MFT-4000, Lanzhou Huahui Instrument Technology, China) with a maximum loading force of 100 N, a length of 5 mm, and a rate of increase of 100 N/min. Each sample was measured three times.

2.3. Friction and wear test

The tribological tests were conducted on a ball-on-disc tribometer (CSM, Switzerland) in rotation mode under a dry sliding condition and lubricated conditions with 0.05 mL of one of the ILs. The counterpart ball was made of 9Cr18 steel and had a diameter of 6 mm. The mode and rotation direction during the test are shown in Fig. 2. The test conditions were as follows: temperature, ~19 °C; relative humidity, ~35%; sliding speed, 300 rev/min (approximately 0.09 m/s); load, 3 N; total sliding distance, 1700 m.

The morphology of the worn surfaces was examined using FE-SEM, and the wear volume was measured on a 3D noncontact surface profiler (MicroXAM-800, KLA-Tencor, USA). The chemical composition of the wear track was evaluated using the EDX analyser. The wear rate was calculated as [19].

$$w = V/NS$$

where w is the wear rate, V is the wear volume, N is the load, and S is the total distance.

3. Results and discussion

3.1. Structure and morphology

3.1.1. SEM investigation results

The surface and cross-sectional morphologies of the two coatings are shown in Fig. 3. The surfaces of both coatings consisted of small, dense particles, as shown in Fig. 3a and c. The cross section of the Cr-GLC coating showed a Cr buffer layer, Cr–C interlayer, and Cr-GLC top layer, all of which were identified using EDX. The Cr buffer layer is composed of pure Cr element. The Cr–C inter layer is composed of Cr and C, and the content of Cr decreases from inside toward outside the buffer layer. The Cr-GLC top layer is composed of 6.81% of Cr and 93.19% of C elements (point A in Fig. 3b). Content in Cr and C were identified using EDX. The cross section of the Cr-DLC coating showed a Cr buffer layer, columnar Cr–C layer, and dense Cr-DLC layer, all of which were identified using EDX. The Cr buffer layer was composed of pure Cr. The columnar Cr–C layer consisted of Cr and C, and the Cr content also decreased gradually from the interior to the exterior. The dense Cr-DLC layer consisted of Cr and C at contents of approximately 6.32% and 93.68%, respectively (point B in Fig. 3d). For accurate analysis of the effects of the structure on the performance, the coating thickness should be as consistent as possible. The thickness of the Cr-GLC coating was 1.91 μm and the thickness of the Cr-DLC coating was 1.92 μm.

3.1.2. AFM investigation results

A good surface morphology is beneficial for tribological behaviour

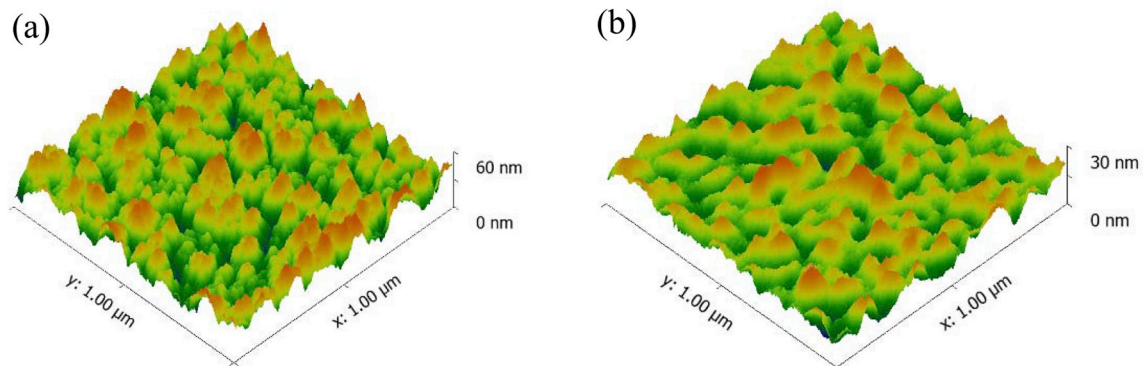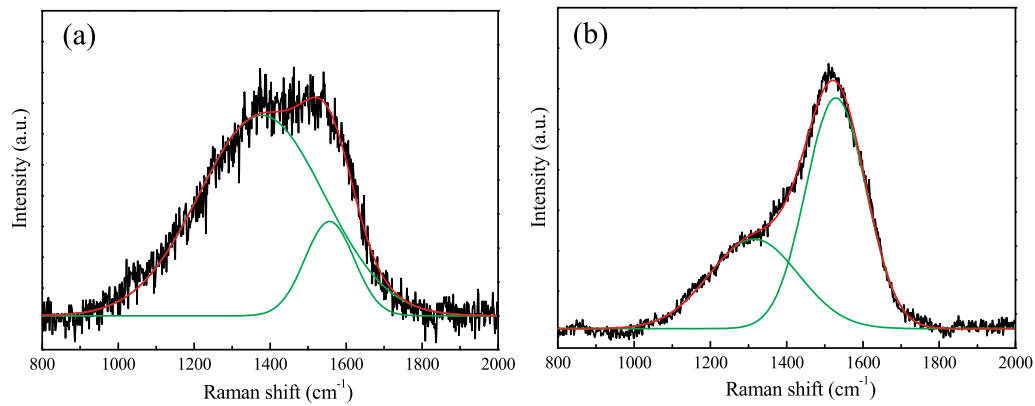**Fig. 4.** AFM images of (a) Cr-GLC surface; (b) Cr-DLC surface.

Fig. 5. Corresponding Raman spectra of (a) Cr-GLC coating; (b) Cr-DLC coating.
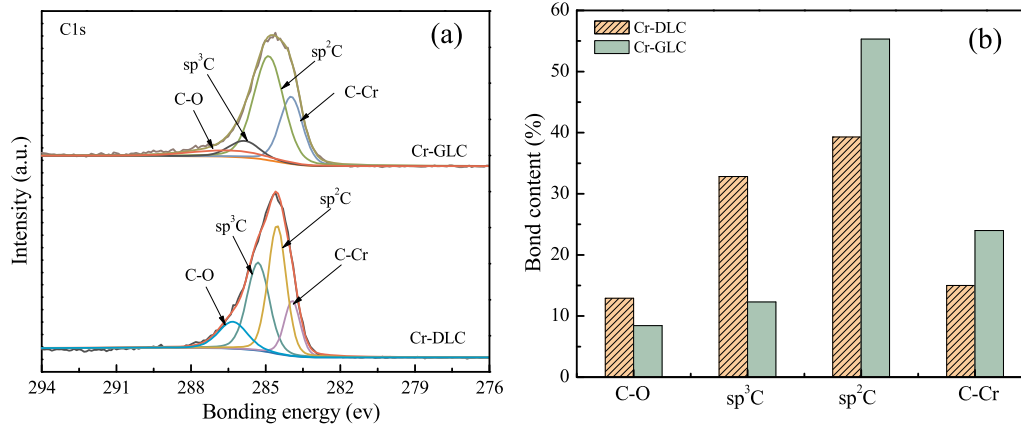

Fig. 6. XPS analysis of (a) C1s peak of Cr-GLC coating and Cr-DLC coating; (b) bond content of Cr-GLC coating and Cr-DLC coating.

[20–22], so it is necessary to analyse the surface morphology. The surface roughness and microstructure of the coatings are shown in Fig. 4. The coatings had dense morphologies, and the particle size distribution was uniform. The surface roughness of the Cr-GLC and Cr-DLC was 6.667 and 0.806 nm, respectively, which indicated that the Cr-DLC coating has a smoother surface. This result is in good agreement with FE-SEM results showing that the Cr-DLC coating is finer than the Cr-GLC coating.

3.1.3. Raman investigation results

The characteristic Raman peaks of the DLC coating are the D peak at 1350 cm^{-1} and the G peak at 1580 cm^{-1} [23], whereas those of the GLC coating are the D peak at 1350 cm^{-1} and G peak at 1560 cm^{-1} [10,24]. Fig. 5 shows the Gaussian-fitted Raman spectra of the coatings. The characteristic D and G peaks of the Cr-GLC coating were located at approximately 1372.9 and 1554.3 cm^{-1}, respectively. However, the D peak and G peak of the Cr-DLC coating appeared at approximately 1310.8 and 1527.2 cm^{-1}, respectively. The G peaks moved towards lower wavenumbers in both coatings compared to their typical G peaks, indicating an increase in disorder in both coatings [25]. The characteristic G peak of the Cr-GLC coating was located at approximately 1554.3 cm^{-1}, and that of the Cr-DLC coating appeared at approximately 1527.2 cm^{-1}. The G peak of the Cr-DLC coating was wider and shifted to a lower wavenumber than that of the Cr-GLC coating owing to increases in the sp^2 C hybrid bond angle disorder and sp^3 C hybrid bonds in the Cr-DLC coating. Both the position and width of the G peak decreased, which is related to selective π-π* resonant Raman scattering of sp^2-bonded carbon clusters of various sizes and the sp^3 fraction of carbon atoms in the coatings [26,27]. The I_D/I_G ratio can qualitatively indicate

the relative content of sp^3 C bonds. The calculated I_D/I_G ratio was approximately 4.81 for the Cr-GLC coating and 0.55 for the Cr-DLC coating, indicating that the Cr-DLC coating has a higher sp^3 C bond content.

3.1.4. XPS investigation results

Both coatings were analysed using XPS to investigate their chemical structure. The C1s level and Lorentzian-Gaussian fitting results of the coatings are shown in Fig. 6a. The C1s peak of the Cr-GLC coating can be fitted by four components, which are centred at approximately 283.8, 284.8, 285.8, and 287 eV and correspond to C–Cr, sp^2 C–C, sp^3 C–C, and C–O bonds [28–30], respectively. The components of the C1s peak of the Cr-DLC coating appeared at 283.9, 284.5, 285.3, and 286.3 eV, and were attributed to the C–Cr, sp^2 C–C, sp^3 C–C, and C–O bonds, respectively. The positions of the sp^2 C and sp^3 C bonds of the Cr-DLC coating were shifted compared with those of the Cr-GLC coating, mainly because of the presence of C–H bonds in the Cr-DLC coating. The presence of C–O bonds in the two coatings may result from oxidation during deposition [31]. The integral area ratios of the sp^2 and sp^3 C bond peaks to the total C1s peak area indicates the content of that type of carbon bond in the coating. The bond contents of the two coatings are shown in Fig. 6b. The ratios of sp^2 C and sp^3 C peaks in the Cr-GLC coating were approximately 55.3% and 12.3%, and those of the sp^2 C and sp^3 C peaks in the Cr-DLC coating were 39.3% and 32.8%, respectively. The results showed that Cr-DLC coating has more sp^3-hybridised carbon bonds, which is consistent with the Raman results. The mechanical properties were affected by the sp^3 C bond content. The hardness of a coating generally increases with increasing sp^3 C bond content [32].
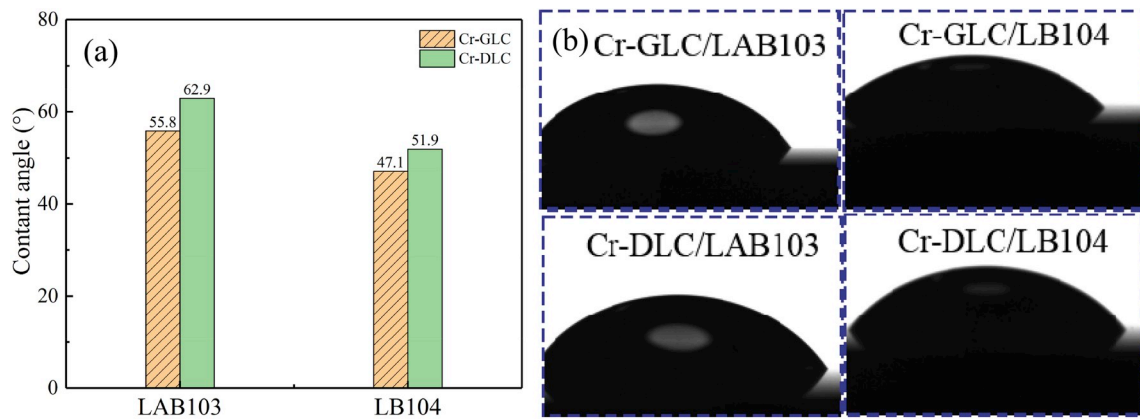
Fig. 7. Contact angles of ILs on the surface of the two coatings.
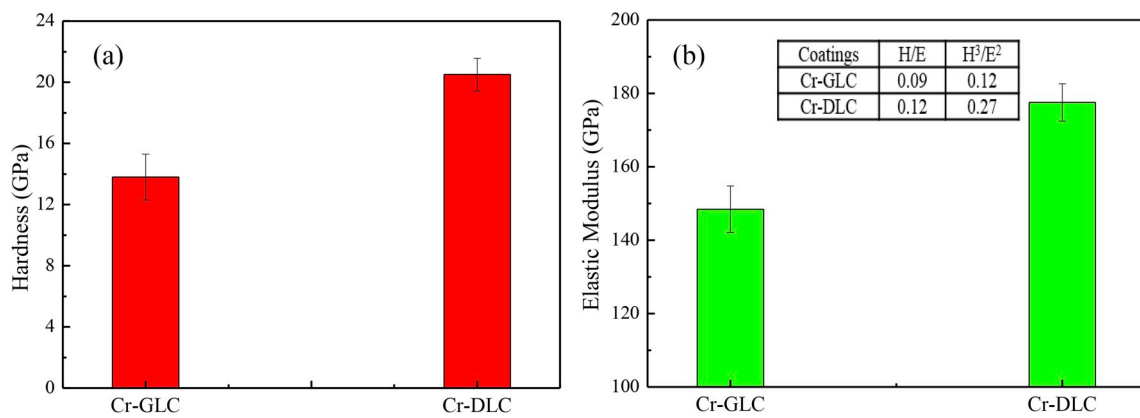

Fig. 8. (a) Hardness of the two coatings; (b) Elastic modulus of the two coatings.
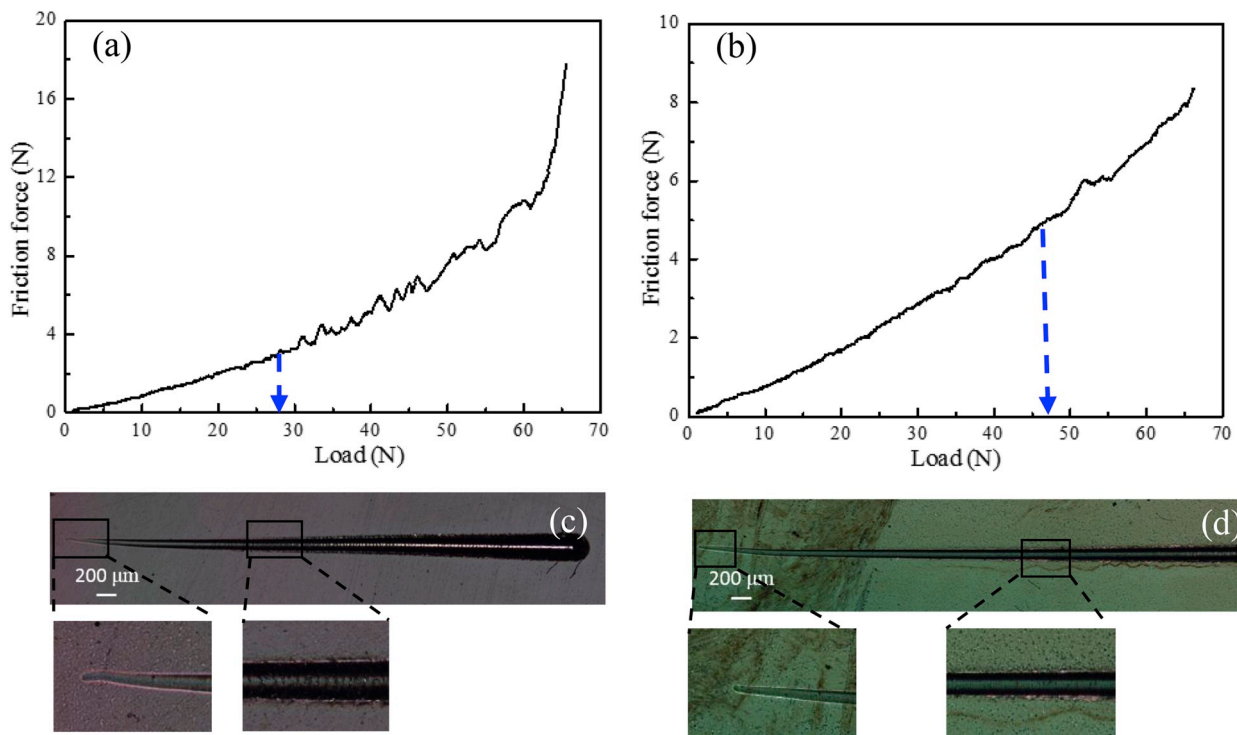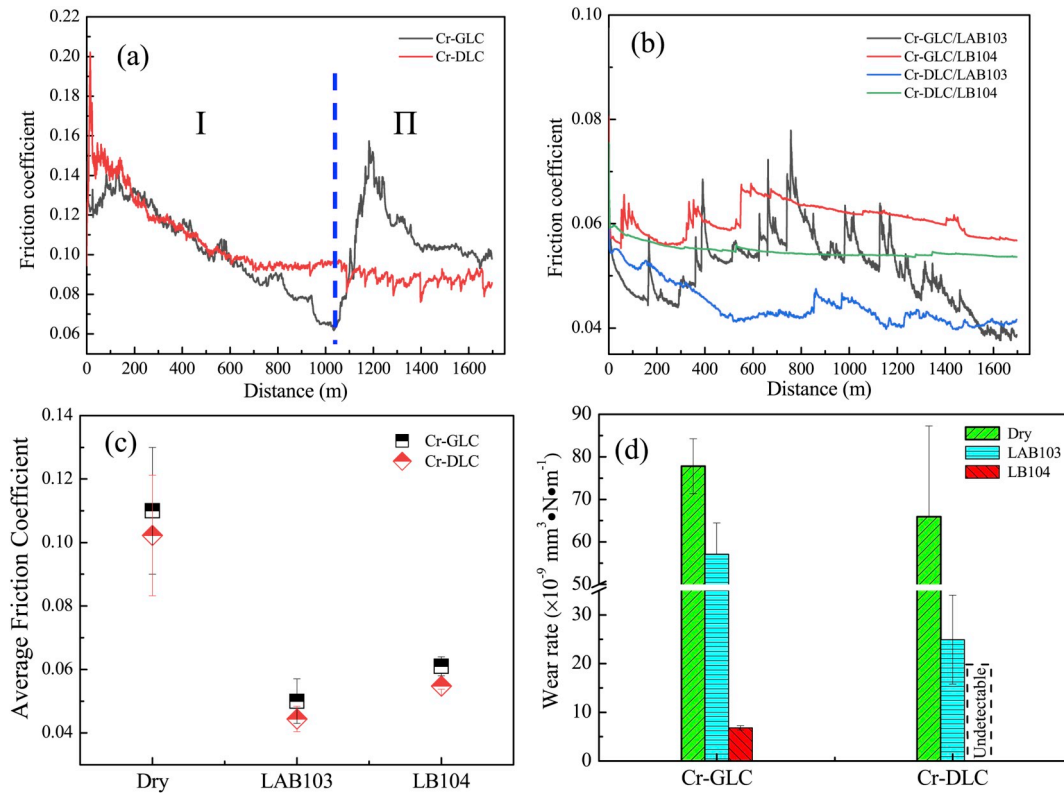

Fig. 9. (a) Friction force curve of Cr-GLC coating during the scratch test; (b) friction force curve of Cr-DLC coating during the scratch test; (c) the optical microscopic image of Cr-GLC coating after the scratch test; (d) the optical microscopic image of Cr-DLC coating after the scratch test.

Fig. 10. Friction and wear properties of coatings: (a) friction coefficient of dry condition; (b) friction coefficient of composite lubrication system; (c) average friction coefficient; (d) wear rate.

3.2. Wettability investigation results

Wettability refers to the ability of a liquid to spread on the surface of a solid. An adsorption film can easily be formed when a liquid has better wettability. The adsorption film can reduce the contact between the friction pairs and thus reduce the friction coefficient. To investigate the cause of the observed differences in the tribological behaviour of the two IL lubricants, the wettability was assessed by measuring the contact angles [33]. Fig. 7 shows the contact angle measurements of each IL on the surfaces of the two coatings. The contact angles of LAB103 on the Cr-GLC and Cr-DLC coatings were 55.8° and 62.9°, and those of LB104 were 47.1° and 51.9°, respectively. A surface with low wettability would generally exhibit a high contact angle. The results showed that LB104 has lower contact angles on the surfaces of both coatings, indicating better wettability. The better wettability of the LB104 lubricant may correspond to a more stable friction coefficient.

3.3. Hardness and elastic modulus investigation results

Coatings typically exhibit good tribological properties when they possess good hardness [34]. To avoid the effect of the matrix, the ratio of the indentation depth and the thickness of each coating is approximately 10% [35]. Fig. 8 shows the hardness (H) and elastic modulus (E) of the two coatings. The hardness and elastic modulus of the Cr-GLC coating were 13.80 and 148.45 GPa, and those of the Cr-DLC coating were 20.50 and 177.54 GPa, respectively. The Cr-DLC coating had a higher hardness and elastic modulus because it had more sp^3 bonds and formed a compact layer. The H/E ratio is directly related to the toughness [36,37]. Specifically, the toughness is proportional to H/E according to formula $K = \delta(P/c^{3/2})$ $(E/H)^{1/2}$ [36], where K is the critical stress intensity for crack propagation. K is not an intrinsic parameter for direct measurement of the toughness; however, it can indicate the magnitude of the toughness. H^3/E^2 characterises a coating's resistance to plastic

deformation [38,39]. The resistance to plastic deformation Py and H^3/E^2 are proportional to each other according to the formula $Py = 0.78r^2$ (H^3/E^2) [39], where r is he contacting sphere radius. The Cr-DLC coating exhibits higher H/E and H^3/E^2 values (Fig. 8b), indicating that it has improved fracture toughness and better resistance to plastic deformation.

3.4. Adhesion force investigation results

The adhesion force between the coating and substrate can reflect the structure and crack resistance of the coating, where a high adhesion force indicates better crack resistance [40,41]. The normal load at which the friction force suddenly changes (that is, the critical separation point of the coating and substrate) indicates the adhesion force [42,43]. The adhesion force of the Cr-GLC coating was approximately 28.6 N, and that of the Cr-DLC coating was approximately 44 N (Fig. 9). This result shows that the Cr-DLC coating has better crack resistance than the Cr-GLC coating.

3.5. Friction and wear properties

3.5.1. Friction coefficient of the dry condition
The friction coefficient versus the sliding distance of each coating under the dry condition is shown in Fig. 10a. The friction coefficient curve of the Cr-GLC coating tested against 9Cr18 steel under the dry condition can be divided into two stages. In the running stage, the friction coefficient of the Cr-GLC coating first increased and then gradually decreased as a transfer film formed. In the second stage, the friction coefficient of the Cr-GLC coating increased sharply and then decreased slowly, possibly because of the effect of furrows in the Cr-GLC coating produced by abrasive particles under friction.

The friction coefficient curve of the Cr-DLC coating under the dry condition decreased gradually up to 700 m, and the curve showed a
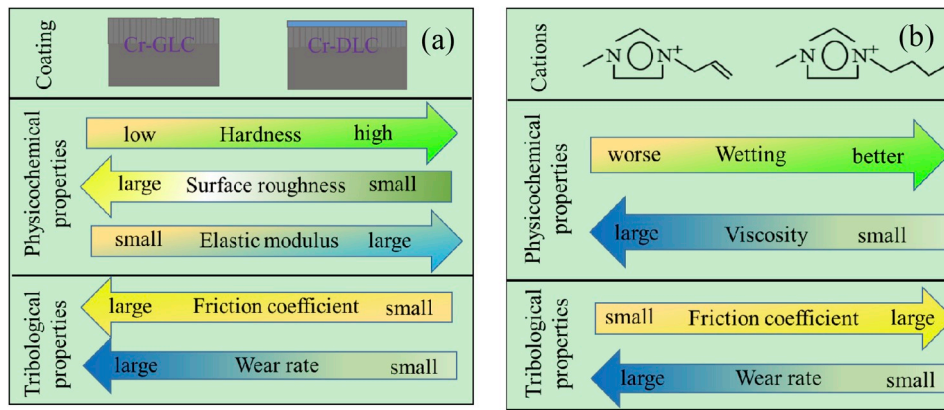
Fig. 11. The relations between the structures and lubricant properties: (a) solid-coatings; (b) ILs.

certain amount of fluctuation with increasing sliding distance. One reason is that it is difficult for the graphitised transfer film to form owing to its higher sp^3 C bond content, which results in a lengthy stage before the friction coefficient becomes stable. Another reason is that the hydrogen in the Cr-DLC coating eliminates the free σ bonds, making it difficult to form C═C bonds and thus reducing the π–π* effect [44]. The friction coefficient of the coating is decreased by surface passivation. The initial friction coefficient of the Cr-GLC coating was much higher than that of the Cr-DLC coating, mainly owing to the large surface roughness of the Cr-GLC coating.

3.5.2. Friction coefficient of the ILs condition

Fig. 10b shows the friction coefficients of the two coatings under IL lubrication. In the Cr-GLC/IL system, the friction coefficient fluctuated, possibly because the chemical reaction film and friction transfer film had mutual influence on the friction pair during the friction process. In addition, the increased roughness of the friction surface caused the curve to fluctuate owing to corrosion of the ILs and the shearing force under friction. By contrast, there was little fluctuation in the Cr-DLC/LAB103 system, mainly because of the dense structure, lower surface roughness and high sp^3 C bond content of the Cr-DLC coating [36]. The Cr-DLC/LB104 composite system had a relatively stable friction coefficient compared to Cr-DLC/LAB103 owing to the superior adsorption
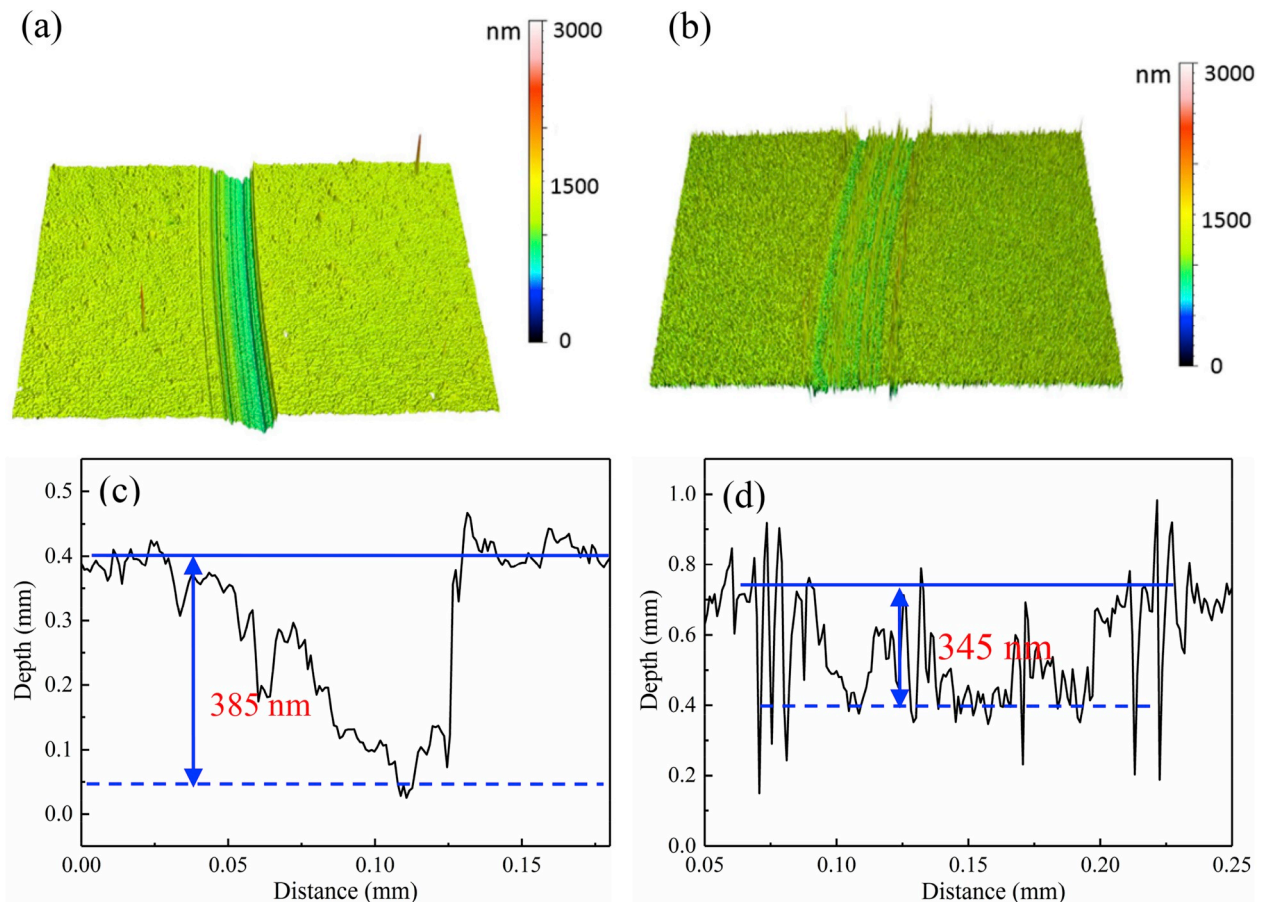

Fig. 12. Worn surfaces at dry condition of (a) Cr-GLC coating 3D topographies; (b) Cr-DLC 3D coating topographies; (c) cross-section of Cr-GLC; (d) cross-section of Cr-DLC.
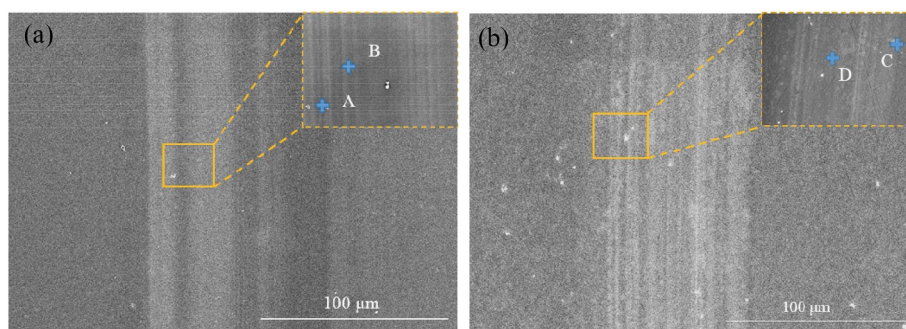
Fig. 13. SEM morphologies at dry condition of (a) Cr-GLC coating wear track; (b) Cr-DLC coating wear track.

film that formed because of the smaller contact angle. In addition, the boundary lubrication film may be more stable in the LB104 system owing to the absence of C=C structure. However, the coefficient of friction of LAB103 was lower than that of LB104 in both the Cr-GLC/IL and Cr-DLC/IL systems. Owing to the higher viscosity, LAB103 supported the formation of a more orderly, thicker film [15].

Fig. 10c shows the average friction coefficient of each coating under different lubrication conditions. The friction coefficients of the two coatings were approximately 0.10 under the dry condition. By contrast, the friction coefficient was approximately 0.045–0.06 for the solid-liquid composite systems, which was approximately 40% lower than that under the dry condition. This is because the surface of the friction pairs can form a good boundary lubrication film and adsorption film when an IL is added. The Cr-DLC coating had a lower average friction coefficient than the Cr-GLC coating under all conditions, mainly because of the passivation effect on the surface of the Cr-DLC coating.

3.5.3. Wear rate

Fig. 10d presents the wear rates of the two coatings under different lubrication conditions. The wear rate of the Cr-DLC coating was lower than that of the Cr-GLC coating under all conditions owing to the higher hardness caused by the high sp^3 C bond content of the Cr-DLC coating. Furthermore, the Cr-DLC coating had higher H/E and H^3/E^2 values, which made crack propagation difficult and improved the anti-wear properties. The wear rate of the Cr-GLC/IL system was 26.67% and 91.25% lower than that under the dry condition for Cr-GLC/LAB103 and Cr-GLC/LB104, respectively. The wear rate decreased by 62.23% for the Cr-DLC/LAB103 system. The results demonstrated that the solid-liquid composite lubrication systems exhibited greatly improved antiwear properties. The reason is probably the passivation of the free σ bonds on the surface of the coatings by the polar radical in the IL [45], which improved the wear resistance. In addition, the friction pairs can form a tribochemical reaction film and an adsorption film when an IL is added to the friction surface, and the films can isolate the wear surfaces and reduce wear. Note that the wear rate was difficult to calculate for the Cr-DLC coating with LB104 lubrication because the wear marks were very light. This can be explained by the high polarity of LB104, which enabled its anion to better react with the steel ball to form a stable tribochemical reaction film and thus reduce wear. Further, the good wettability of LB104 is also advantageous for reducing the wear rate [45]. To summarise the above results, the lubrication behaviour of the solid-liquid composite lubrication systems was affected by the physicochemical properties of the ILs and coatings. The relationship between the structure and tribological properties is illustrated in Fig. 11.

4. Discussion

4.1. Wear mechanism of the two coatings tested against 9Cr18 in dry condition

To clearly observe the wear surface, the 3D topography and FE-SEM

Table 2
EDX results of the wear track and debris.

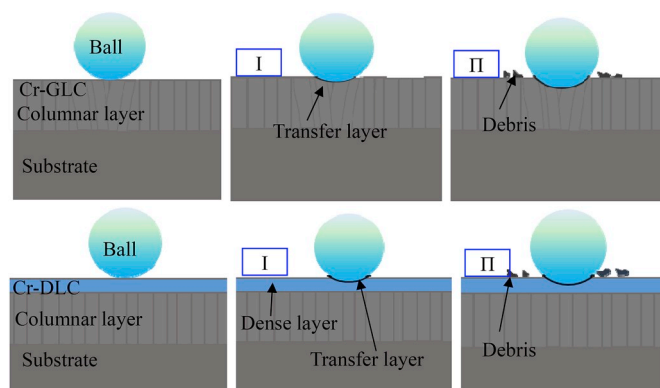| Point	C (at. %)	O (at. %)	Fe (at. %)	Cr (at. %)
A	68.4	9.36	9.34	9.57
B	74.64	1.61	14.76	8.99
C	65.13	4.00	0.48	30.40
D	65.16	4.42	30.13	0.28

Fig. 14. Schematic diagram of wear mechanism of the two coatings with dry condition.

morphology were characterised. Fig. 12 shows the 3D topography and cross-sectional profiles of the two coatings under the dry condition. Many deep furrows appear in the wear track of the Cr-GLC coating, indicating that the sharp increase in the friction coefficient was caused by the furrow effect. The wear track of the Cr-DLC coating shows wear debris and furrows (Fig. 12b). The depth and width of the wear track of the Cr-GLC coating are both larger than those of the Cr-DLC coating, as shown in the cross-sectional profiles in Fig. 12c and d. The reason is that hard particles from the steel ball can form deep furrows by the action of the shear force during sliding owing to the lower hardness of the Cr-GLC coating. Furthermore, more sp^2 C bonds, which mainly composed of large number of nano-graphite and graphite-like clusters [46], could facilitate the formation of graphitised transfer films. By contrast, more wear debris and fewer furrows were produced in the Cr-DLC coating owing to its higher hardness. The presence of furrows on the wear track indicated that the main wear mechanism for the two coatings is abrasive wear.

Large amounts of debris and furrows on the surfaces of the two coatings were observed in the FE-SEM morphologies, and the Cr-DLC coating generated more debris, as shown in Fig. 13a and Fig. 13b. Table 2 shows the chemical composition of the debris and wear scars. In addition to C and Cr, a higher Fe content was detected in the Cr-GLC coating, which was probably derived from wear debris from the ball
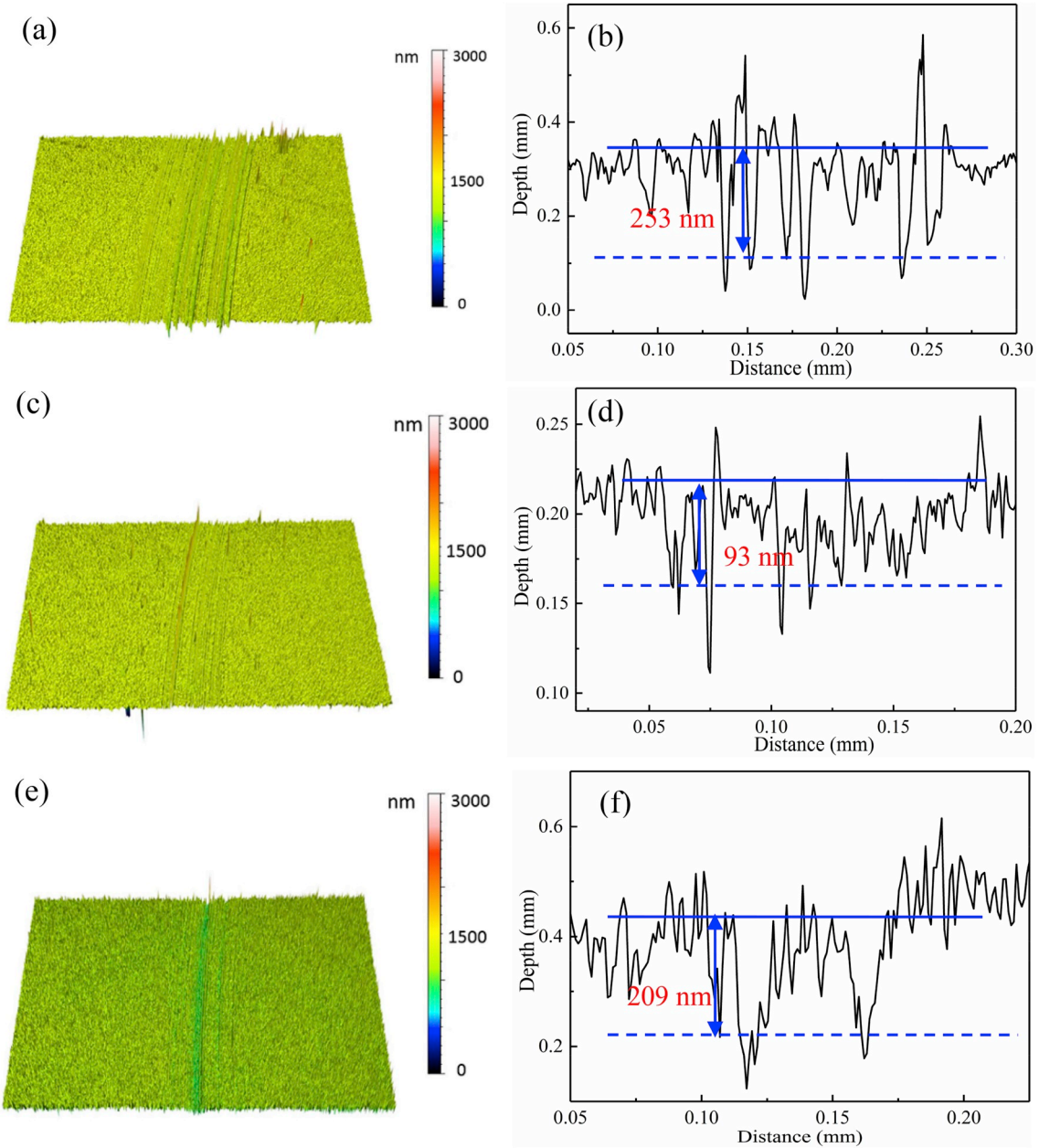
Fig. 15. Worn surfaces at ILs condition of (a) Cr-GLC/LAB103 3D topographies; (b) cross-section of Cr-GLC/LAB103; (c) Cr-GLC/LB104 3D topographies; (d) cross-section of Cr-GLC/LB104; (e) Cr-DLC/LAB103 3D topographies; (f) cross-section of Cr-DLC/LAB103.

embedded in the wear track. Both coatings contained some O, which may result from the chemical reaction of the friction pair with the oxygen under friction [47]. A schematic diagram of the wear mechanism of the two coatings is shown in Fig. 14.
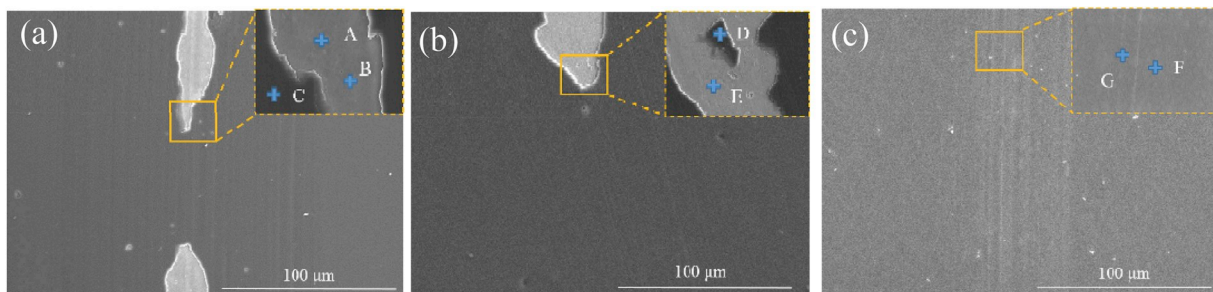

Fig. 16. SEM morphologies at ILs condition of (a) Cr-GLC/LAB103 system wear track; (b) Cr-GLC/LB104 system wear track; (c) Cr-DLC/LAB103 system wear track.
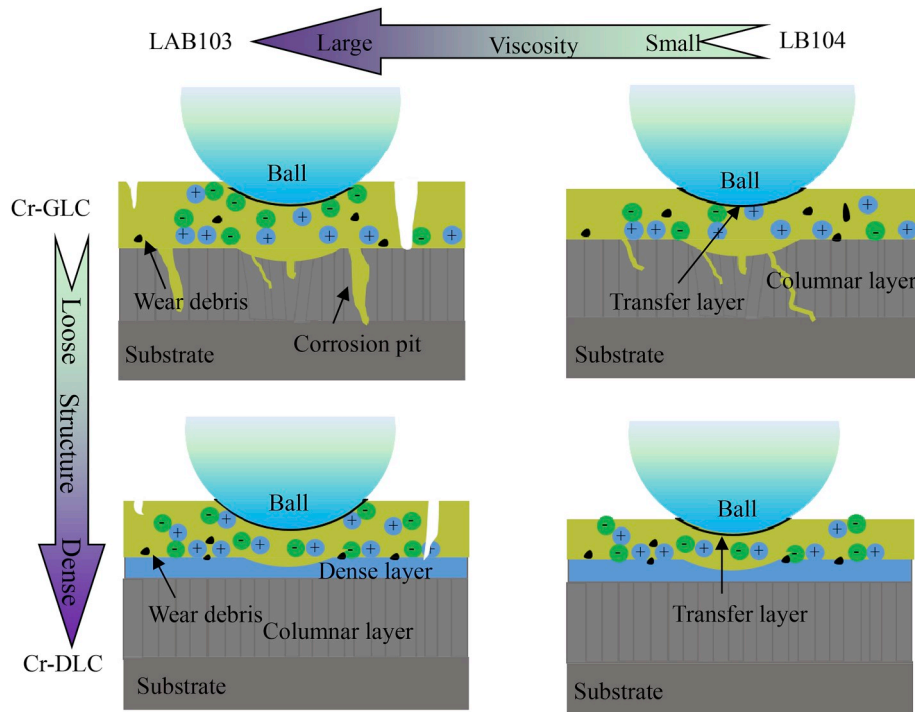
Fig. 17. Schematic diagram of wear mechanism of the two coatings with ILs.

Table 3
EDX results of the wear track and debris.

Point	B (at. %)	C (at. %)	N (at. %)	O (at. %)	F (at. %)	Cr (at. %)	Fe (at. %)
A		69.02	0.98	3.74	1.06	18.42	8.43
B	4.33	9.62	0.43	0.45	2.75	15.75	66.67
C		80.38	1.17	0.72		14.20	13.19
D		74.88		0.89		9.52	14.71
E		11.64			4.10	14.62	68.34
F		63.97	0.47	7.49	0.38	27.45	0.23
G		66.21				33.43	0.36

4.2. Wear mechanism of the two coatings tested against 9Cr18 under ionic liquid lubrication condition

The 3D topographies and cross-sectional profiles of the two coatings under lubrication by each IL are shown in Fig. 15. Obvious furrows and protrusions were observed in the wear track of the Cr-GLC/LAB103 system, and some shallow grooves appeared in the Cr-GLC/LB104 system. A comparison of the depths of the wear tracks under all conditions revealed that the tracks were deepest under the dry condition and shallowest under lubrication by LB104, indicating that the wear resistance can be effectively improved by using a solid-liquid composite lubrication system. The reason are as follows. First, the coating exhibited good boundary lubrication when the ILs were added, which is beneficial for decreasing the wear. Second, the addition of the IL can effectively enhance the plastic deformation resistance, which can reduce the shear force and improve the antiwear properties [48]. Finally, the free σ bonds on the surface of the Cr-GLC coating can react with ions in the IL to generate a covalent bond structure and thus reduce wear [16]. The wear track in the LAB103-containing system was deeper than that in the LB104-containing system, which can be attributed to the continuous and stable isolation film favoured by the better wettability of LB104 for the Cr-GLC coating.

The FE-SEM morphology of the Cr-GLC coating under lubrication by each IL is shown in Fig. 16. In addition to shallow grooves, discontinuous debris from massive spallation and wear debris also appeared in the solid-liquid composite lubrication system. The reason is that the corrosive IL may penetrate the coating through the coarse columnar structure, which can cause massive spallation in combination with the friction shear effect. A schematic diagram of the corrosion and wear in the Cr-GLC/IL systems is shown in Fig. 17. The chemical composition is shown in Table 3; points B and E both showed a high Fe content, which indicated that the coating was broken. The presence of O, Fe, and other elements, which indicates that a tribochemical reaction occurred during sliding, can reduce wear [18]. The antiwear performance of LB104 was better than that of LAB103 owing to the poor shear resistance of LAB103 resulting from the C=C structure. By contrast, the adsorption film of LB104 was stable, and the anion in LB104 was more likely to react with the steel ball to form fluoride owing to the high polarity, which can further reduce wear.

A comparison of the Cr-GLC and Cr-DLC coatings under LAB103 lubrication showed that the wear track of the Cr-GLC coating was wider and had more obvious furrows. The presence of the furrows indicated that abrasive wear occurred in both coatings under LAB103 lubrication. Both coatings showed no obvious plastic deformation, indicating that boundary lubrication and solid lubrication in the solid-liquid composite lubrication systems had a good synergistic effect [49]. The depth of the wear tracks showed that the Cr-DLC/IL systems had a better composite lubrication effect. A schematic diagram of the Cr-DLC/IL systems is shown in Fig. 17. As indicated by the FE-SEM morphologies, more wear debris and almost no massive spallation were observed in the Cr-DLC coating. The reason is the lower hardness of Cr-GLC caused by the presence of more sp² C bonds, which reduced the shear resistance. In addition, the IL can pass through the columnar structure of the Cr-GLC coating more easily, which can weaken the bonding force for the corrosion effect and thus reduce the wear resistance of the coating. However, the dense layer of the Cr-DLC coating can effectively resist the corrosive effects of the ILs, ensuring superior tribological performance.

5. Conclusions

In this study, the mechanical and tribological properties of Cr-GLC and Cr-DLC coatings under lubrication using different ILs were

investigated. The following conclusions were drawn:

The prepared Cr-GLC and Cr-DLC coatings both exhibited good adhesion force to the substrate, as well as good mechanical properties, and the dense layer in the Cr-DLC coating contributed to the improvement in the mechanical properties.

Both coatings exhibited better antifriction and antiwear effects in the solid-liquid composite lubrication systems, and the better synergistic lubrication effect was explained. The lubrication effect of the ILs was closely related to their viscosity and wettability. LAB103 showed a better antifriction effect, and LB104 exhibited a better antiwear effect.

The Cr-GLC/IL systems were strongly affected by the corrosive effect of the IL, whereas the Cr-DLC/IL systems were barely affected. Abrasive wear was the main wear mechanism in the Cr-DLC/IL composite lubrication systems, whereas abrasive wear and corrosion wear were both involved in the Cr-GLC/IL systems.

Declaration of competing interest

All the authors declare no competing financial interest for this paper.

Acknowledgments

References

[1] Casiraghi C, Robertson J, Ferrari AC. Diamond-like carbon for data and beer storage. Mater Today 2007;10:44–53.

[2] Chu PK, Li L. Characterization of amorphous and nanocrystalline carbon films. Mater Chem Phys 2006;96:253–77.

[3] Qiang L, Gao K, Zhang L, Wang J, Zhang B, Zhang J. Further improving the mechanical and tribological properties of low content Ti-doped DLC film by W incorporating. Appl Surf Sci 2015;353:522–9.

[4] Masuko M, Ono T, Aoki S, Suzuki A, Ito H. Friction and wear characteristics of DLC coatings with different hydrogen content lubricated with several Mo-containing compounds and their related compounds. Tribol Int 2015;82:350–7.

[5] Ronkainen H, Varjus S, Holmberg K. Friction and wear properties in dry, water and oil-lubricated DLC against alumina and DLC against steel contacts. Wear 1998;222:120–8.

[6] Donet C, Belin M, Auge J, Martin J, Grill A, Patel V. Tribochemistry of diamond-like carbon coatings in various environments. Surf Coat Technol 1994;68–69:626–31.

[7] Wang Y, Wang L, Xue Q. Improvement in the tribological performances of Si₃N₄, SiC and WC by graphite-like carbon films under dry and water-lubricated sliding conditions. Surf Coat Technol 2011;205:2770–7.

[8] Wang L, Guan X, Zhang G. Friction and wear behaviors of carbon based multilayer coatings sliding against different rubbers in water environment. Tribol Int 2013;64:69–77.

[9] Field S, Jarratt M, Teer D. Tribological properties of graphite-like and diamond-like carbon coatings. Tribol Int 2004;37:949–56.

[10] Li Z, Guan X, Wang Y, Li J, Cheng X, Lu X, Wang L, Xue Q. Comparative study on the load carrying capacities of DLC, GLC and CrN coatings under sliding-friction condition in different environments. Surf Coat Technol 2017;321:350–7.

[11] Aboua K, Umehara N, Kousaka H, Deng X, Tasdemirb H, Mabuchi Y, Higuchi T, Kawaguchi M. Effect of carbon diffusion on friction and wear properties of diamond-like carbon in boundary base oil lubrication. Tribol Int 2017;113:389–98.

[12] Aboua K, Umehara N, Kousaka H, Tokoroyama T, Murashima M, Mabuchi Y, Higuchi T, Kawaguchi M. Effect of carbon diffusion on friction and wear behaviors of diamond-like carbon coating against germanium in boundary base oil lubrication. Tribol lett 2019;2:65–7.

[13] Fan X, Wang L, Li W, Wan S. Improving tribological properties of multialkylated cyclopentanes under simulated space environment: two feasible approaches. ACS Appl Mater Interfaces 2015;7:14359–68.

[14] Zhuang W, Fan X, Li W, Li H, Zhang L, Peng J, Cai Z, Mo J, Zhang G, Zhu M. Comparing space adaptability of diamond-like carbon and molybdenum disulfide films toward synergistic lubrication. Carbon 2018;134:163–73.

[15] Somers A, Howlett P, MacFarlane D, Forsyth M. A review of ionic liquid lubricants. Lubricants 2013;1:3–21.

[16] Feng X, Xia Y. Tribological properties of Ti-doped DLC coatings under ionic liquids lubricated conditions. Appl Surf Sci 2012;258:2433–8.

[17] Tariq M, Serro A, Colaco R, Saramago B, Lopes J, Rebelo L. Effect of alkyl chain length on the adsorption and frictional behaviour of 1-alkyl-3-methylimidazolium chloride ionic liquid surfactants on gold surfaces. Colloids Surf, A 2011;377(1–3):361–6.

[18] Yao M, Fan M, Liang Y, Zhou F, Xia Y. Imidazolium hexafluorophosphate ionic liquids as high temperature lubricants for steel-steel contacts. Wear 2010;268:67–71.

[19] Sui X, Liu J, Zhang S, Yang J, Hao J. Microstructure, mechanical and tribological characterization of CrN/DLC/Cr-DLC multilayer coating with improved adhesive wear resistance. Appl Surf Sci 2018;439:24–32.

[20] Wei C, Yang J. A finite element analysis of the effects of residual stress, substrate roughness and non-uniform stress distribution on the mechanical properties of diamond-like carbon films. Diam Relat Mater 2011;20:839–44.

[21] Jo Y, Zhang T, Son M, Kim K. Synthesis and electrochemical properties of Ti-doped DLC films by a hybrid PVD/PECVD process. Appl Surf Sci 2018;433:1184–91.

[22] Khalaj Z, Ghoranneviss M, Vaghri E, Saghaleini A, Diudea MV. Deposition of DLC film on stainless steel substrates coated by nickel using PECVD method. Acta Chim Slov 2012;59:338.

[23] Ebrahimi M, Mahboubi F, Naimi-Jamal M. Wear behavior of DLC film on plasma nitrocarburized AISI 4140 steel by pulsed DC PACVD: effect of nitrocarburizing temperature. Diam Relat Mater 2015;52:32–7.

[24] Dong D, Jiang B, Li H, Du Y, Yang C. Effect of graphite target power density on tribological properties of graphite-like carbon films. Appl Surf Sci 2018;439:900–9.

[25] Ferrari A, Robertson J. Interpretation of Raman spectra of disordered and amorphous carbon. Phys Rev B 2000;61:14095–107.

[26] Ferrari A, Robertson J. Resonant Raman spectroscopy of disordered, amorphous, and diamond like carbon. Phys Rev B: Condens Matter 2001;64:075414.

[27] Shi J, Shi X, Sun Z, Lau S, Tay B, Tan H. Resonant Raman studies of tetrahedral amorphous carbon films. Diam Relat Mater 2001;10:76–81.

[28] Wu D, Ren S, Pu J, Lu Z, Zhang G, Wang L. A comparative study of tribological characteristics of hydrogenated DLC film sliding against ceramic mating materials for helium applications. Appl Surf Sci 2018;441:884–94.

[29] Paik N. Raman and XPS studies of DLC films prepared by a magnetron sputter-type negative ion source. Surf Coat Technol 2005;200:2170–4.

[30] Sun J, Fu Z, Zhang W, Wang C, Yue W, Lin S, Dai M. Friction and wear of Cr-doped DLC films under different lubrication conditions. Vacuum 2013;94:1–5.

[31] Tokoroyama T, Hattori T, Umehara N, Kousaka H, Manabe K, Kishi M, Fuwa Y. Ultra-low friction properties of carbon nitride tantalum coatings in the atmosphere. Tribol Int 2016;103:388–93.

[32] Su F, Chen G, Sun J. Synthesis of hydrogenated DLC film by PECVD and its tribocorrosion behaviors under the lubricating condition of graphene oxide dispersed in water. Tribol Int 2019;130:1–8.

[33] Qi J, Wang L, Yan F, Xue Q. The tribological performance of DLC-based coating under the solid–liquid lubrication system with sand-dust particles. Wear 2013;297:972–85.

[34] Duminica F, Belchi R, Libralesso L, Mercier D. Investigation of Cr(N)/DLC multilayer coatings elaborated by PVD for high wear resistance and low friction applications. Surf Coat Technol 2018;33:396–403.

[35] Cao Z, Xia Y, Liu L, Feng X. Study on the conductive and tribological properties of copper sliding electrical contacts lubricated by ionic liquids. Tribol Int 2019;130:27–35.

[36] Zhang S, Zhang X. Toughness evaluation of hard coatings and thin films. Thin Solid Films 2012;520:2375–89.

[37] Bai W, Li L, Xie Y, Liu D, Wang X, Jin G, Tu J. Corrosion and tribocorrosion performance of M (M_Ta, Ti) doped amorphous carbon multilayers in Hank's solution. Surf Coat Technol 2016;305:11–22.

[38] He D, Shang L, Lu Z, Zhang G, Wang L, Xue Q. Tailoring the mechanical and tribological properties of B₄C/a-C coatings by controlling the boron carbide content. Surf Coat Technol 2017;329:11–8.

[39] Leyland A, Matthews A. On the significance of the H/E ratio in wear control: a nanocomposite coating approach to optimised tribological behavior. Wear 2000;246:1–11.

[40] Neuville S. Quantum electronic mechanisms of atomic rearrangements during growth of hard carbon films. Surf Coat Technol 2011;206:703–26.

[41] Ye Y, Wang Y, Chen H, Li J, Yao Y, Wang C. Doping carbon to improve the tribological performance of CrN coatings in seawater. Tribol Int 2015;90:362–71.

[42] Hua C, Guo J, Liu J, Yan X, Zhao Y, Chen L, Wei J, Hei L, Li C. Influence of diamond surface chemical states on the adhesion strength between Y₂O₃ film and diamond substrate. Mater Des 2016;105:81–8.

[43] Yao J, Lv L, He Y, Wang D. Size effect of (Al₂O₃-Y₂O₃)/YSZ micro-laminated coating on high-temperature oxidation resistance. Appl Surf Sci 2013;279:85–91.

[44] Erdemir A. The role of hydrogen in tribological properties of diamond-like carbon films. Surf Coat Technol 2001;146:292–7.

[45] Huang J, Wan S, Wang L, Xue Q. Tribological properties of Si-doped graphite-like amorphous carbon film of PEEK rubbing with different counterparts in SBF medium. Tribol Lett 2015;57:10.

[46] Gilewicz A, Warcholinski B. Tribological properties of CrCN/CrN multilayer coatings. Tribol Int 2014;80:34–40.

[47] Zhang H, Endrino J, Anders A. Comparative surface and nano-tribological characteristics of nanocomposite diamond-like carbon thin films doped by silver. Appl Surf Sci 2008;255:2551–6.

[48] Han Y, Qiao D, Zhang S, Feng D. Influence of phosphate and phosphonate ionic liquid structures on lubrication for different alloys (Mg, Al, Cu). Tribol Int 2017;114:469–77.

[49] Liu X, Pu J, Wang L, Xue Q. Novel DLC/ionic liquid/graphene nanocomposite coatings towards high-vacuum related space applications. J Mater ChemaA 2013;1:3797–809.